Ecotoxicology and Environmental Safety 307 (2025) 119426

Contents lists available at ScienceDirect

Ecotoxicology and Environmental Safety

journal homepage: www.elsevier.com/locate/ecoenv

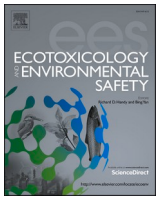

Genomic variation in *Saccharomyces cerevisiae* influences paraquat response through differential oxidative stress and vacuolar adaptations

Juan Carlos Rubilar [a,1], Benjamín Szenfeld [a], Francisco A. Cubillos [b,c,d], Andrés. D. Klein [a,*]

[a] Centro de Genética y Genómica, Facultad de Medicina, Clínica Alemana Universidad del Desarrollo, Santiago 7780272, Chile
[b] Departamento de Biología, Facultad de Química y Biología, Universidad de Santiago de Chile, Santiago, Chile
[c] Millennium Institute for Integrative Biology (iBio), Santiago, Chile
[d] Millenium Nucleus of Patagonian Limit of Life (LiLi), Santiago, Chile

ARTICLE INFO

Edited by Richard Handy

Keywords:
Paraquat
Saccharomyces cerevisiae
Parkinson's disease
Herbicide
Pollution

ABSTRACT

The conserved genetics between *Saccharomyces cerevisiae* and mammals makes yeast an ideal model for studying the biological effects of paraquat (PQ), an herbicide linked to Parkinson's disease (PD) risk in humans. To determine how genetic background influences PQ toxicity, we treated four diverse yeast strains (NA, SA, WA, and WE) and assessed their physiological (growth curves), molecular (superoxide and peroxide levels), and cellular (vacuolar morphology/disaggregation) responses. PQ significantly reduced the specific growth rate (μMax) in WE and WA strains, while SA and NA remained unaffected. Superoxide and peroxide levels increased across all strains to varying degrees, with SA and WE exhibiting the highest accumulation. Furthermore, we found an inverse association between superoxide levels and μMax. PQ also induced strain-dependent vacuolar morphology shifts, from a single large organelle to fragmented vacuoles, with the susceptible WE strain displaying the most extreme disaggregation. Given the known link between lysosomal dysfunction and pesticide-induced PD, we investigated correlations between predicted missense variants in vacuolar genes and PQ responses. This analysis identified associations between *fen2* variants, the human *SLC17A5* ortholog, and vacuolar disaggregation. Validation using a *fen2*-deleted strain (*Δfen2*) confirmed its mechanistic role, showing increased vacuolar fragmentation, elevated oxidative markers, and compromised growth upon PQ exposure. In conclusion, our findings demonstrate that PQ susceptibility is intrinsically linked to intracellular superoxide levels and that *fen2* plays a critical role in the vacuolar adaptive response to oxidative stress. The mechanisms employed by the most resistant strains may inform the development of novel therapeutics for PQ-exposed individuals.

1. Introduction

Paraquat (PQ) is a potent herbicide employed globally for its efficacy in eradicating crop-detrimental organisms. Despite its widespread application, with an estimated global consumption of $3.5 million tons annually (Pretty and Bharucha, 2015), PQ poisoning is responsible for approximately ~20,000 deaths yearly (Ball et al., 2019). Furthermore, a clear link between PQ exposure and an increased risk of Parkinson's disease (PD) has been established, raising serious environmental and human health concerns (Paul et al., 2024).

The pathogenesis PD is complex, and the precise etiology of most cases remains unknown. However, development is consistently attributed to a complex interplay between genetic and environmental factors. Multiple PD genetic risk factors are known to interact with pesticide and herbicide exposure (Fleming, 2017). Nevertheless, the precise molecular mechanisms of gene-environment (GxE) interaction remain elusive. Elucidating these mechanisms is essential for achieving early diagnosis, developing preventative strategies, and translating potential therapeutic interventions (Burbulla and Krüger, 2011).

PQ exerts its toxicity by inhibiting mitochondrial Complex I through the reduction of NADH-cytochrome b5 and NADH-ubiquinone oxidoreductases. This process elevates superoxide anion ($O_2^{\cdot-}$) levels, which are subsequently converted into highly reactive species like hydrogen peroxide (H_2O_2) and hydroxyl radicals (HO.) (Hernandez-Baixauli et al.,

* Corresponding author.
E-mail address: andresklein@udd.cl (Andrés.D. Klein).
[1] Present address: Team DNA Damage and Genome Instability. Cancer Research Center of Marseille (CRCM), CNRS, Aix Marseille University, Inserm, Institut Paoli-Calmettes, Marseille 13009, France.

https://doi.org/10.1016/j.ecoenv.2025.119426
Received 14 May 2025; Received in revised form 12 November 2025; Accepted 13 November 2025
Available online 18 November 2025

2024). Additionally, PQ induces the mitochondrial permeability transition pore (mPTP) opening, which reduces intra-mitochondrial calcium retention capacity and decreases the membrane potential, further contributing to increased Reactive Oxygen Species (ROS) levels (See et al., 2022). This mitochondrial damage directly impacts the lysosomal pathway via membrane contact sites, resulting in decreased lysosomal enzyme activities, impaired sphingolipid degradation, and blockage of autophagy (Rubilar et al., 2024). These sequential disruptions contribute to alpha-synuclein (α-syn) aggregation, dopaminergic neuron death, and eventual motor impairments (Klein and Mazzulli, 2018).

Yeast models (*S. cerevisiae*) have emerged as an invaluable resource for dissecting the underlying genetic and molecular mechanisms of PD pathogenesis. This utility stems from yeast's high degree of evolutionary conservation with humans, rapid growth and generation time, the availability of genetically diverse strain panels, and the capacity for high-throughput characterization and implementation of large-scale deletion studies (Mülleder et al., 2012). Mechanistic insights derived from this simple model are highly translatable to human PD, exemplified by studies where the yeast internal NADH-quinone oxidoreductase (NDI1) was successfully used as a gene therapy candidate to restore defective mitochondrial Complex I function in mammalian PD models (Li et al., 2022).

In this study, we investigated the biological effects of PQ exposure on four *S. cerevisiae* strains with distinct genetic backgrounds. We employed a multi-tiered approach, examining the consequences at the physiological (growth rates), molecular (ROS levels), and cellular (vacuolar morphology) levels, and the interplay between them. This comprehensive strategy is designed to provide mechanistic insights into GxE interactions, potentially elucidating genetic factors that influence PD susceptibility and advancing the identification of novel therapeutic strategies.

2. Results

2.1. Paraquat-induced strain-specific growth rates responses

We chose four phylogenetically distinct strains exhibiting extensive genomic variability, whose genomes are sequenced: Y12 (Sake, SA), YPS128 (North American, NA), DBVPG6044 (West African, WA) and DBVPG6765 (Wine/European, WE). As a proxy of cell health, we measured their growth rates under control and PQ exposure. Initially, we set the lowest PQ concentration, which induced reproducible variation across strains. We tested a range of 25–125 μg/mL (Supplementary Figure 1) and chose 75 μg/mL to discriminate between strains. Under control conditions (YNB media 2 % glucose) all strains exhibited similar growth patterns (Fig. 1A). However, upon PQ exposure we identified a lower growth rate in the WE background than untreated cells (susceptibility phenotype) (Fig. 1B). This effect was quantified by calculating the Area Under the Curve (AUC) (p-value = 0.0013, ANOVA) (Fig. 1C). Conversely, SA, NA and WA exhibit the highest tolerance to PQ (resistance phenotype, p-value = ns, ANOVA) (Fig. 1B and C).

From the growth curves, we calculated μMax, which corresponds to the maximum rate at which the yeast can increase its population size as another proxy of reproductive fitness. PQ exposure differentially impacted μMax across the strains. PQ-treated WE exhibited a decrease in μMax compared to NA (p-value = 0.0012, ANOVA) (Fig. 1D). Notably, the WE strain exhibited a 40 % reduction in μMax compared to SA (p-value = 0.0001, ANOVA), with WA showing a 20 % decrease when compared to SA (p-value = 0.033, ANOVA) (Fig. 1D). Furthermore, we found a significant difference between WA and WE (p-value = 0.033,

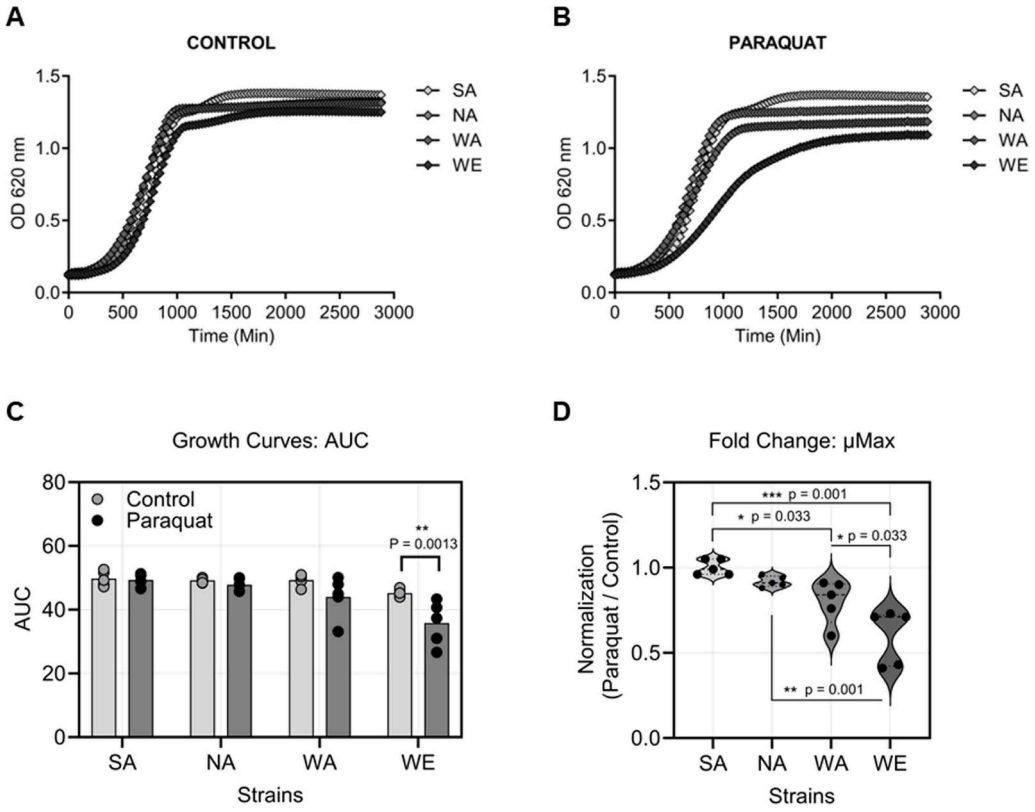

Fig. 1. Reproductive fitness of *S. cerevisiae* parental strains following PQ exposure. (A) Growth curves of SA, NA, WA, and WE strains under control conditions. (B) Growth curves after PQ exposure (75 μg/mL). (C) Average Area Under the Curve (AUC). (D) Average fold change of μMax (PQ/mock). Biological replicates (N = 5). Data are presented as mean ± SE. Statistical tests: Shapiro-Wilk for normality (p-value > 0.05), ANOVA test p-value < 0.05, post-hoc Holm-Sidak (AUC and fold change). Statistical significance indicated by asterisks: p-value ≤ 0.05 (*), p-value < 0.01 (**), p-value < 0.001 (***), p-value < 0.0001 (****), ns = not significant (p-value > 0.05). Statistical analysis was performed using SPSS v20.0 and plotted using GraphPad.

ANOVA). These results demonstrate that PQ differentially impacts each strain, with WE and WA exhibiting the most significant susceptibility. Therefore, PQ exposure has a strain-specific impact on yeast reproductive fitness and physiological adaptation.

2.2. PQ induced strain-specific ROS responses

Given that PQ inhibits mitochondrial complex I, we analyzed superoxide anion levels with DHE, under control and PQ treatments (75 μg/mL for 48-hours) by microscopy. Under control conditions, we found no visible oxidation of the probe (Fig. 2A). Upon PQ exposure, oxidized DHE binds to DNA, emitting visible red fluorescence (Fig. 2A). All PQ-treated strains exhibited probe oxidation (red fluorescence). Interestingly, the NA strain exhibited lower fluorescence intensity compared to WA (p-value = 0.0265, ANOVA) and WE (p-value = 0.0027, ANOVA) (Fig. 2B). Similarly, the SA strain showed lower intensity fluorescence compared to WA (p-value = 0.0092, ANOVA) and WE (p-value = 0.0011, ANOVA) (Fig. 2B), indicating lower oxidative stress levels in these strains when were exposed to PQ (Fig. 2B). In addition, PQ exposure induced significant changes in hydrogen peroxide levels when compared to control conditions (Fig. 2C). Furthermore, significant differences in DCF fluorescence rates were observed among strains SA and WA after PQ treatment (p-value = 0.0279, ANOVA) (Fig. 2D). These results indicate that PQ differentially impacts the yeast strains superoxide anion and hydrogen peroxide levels across yeast strains, providing molecular-level insights into the oxidative stress induced by PQ exposure.

2.3. PQ induced strain-specific vacuolar adaptations

To investigate how yeast strains adapt to PQ exposure, we examined their vacuolar morphology, as changes in vacuole structure often indicate activation of stress response mechanisms (Saldaña et al., 2021). Vacuoles are typically classified into three phenotypes: A, up to three large vacuoles per cell; B, multiple small vacuoles with defined borders, and C, highly fragmented vacuoles (Fig. 3A) (Aufschnaiter and Büttner, 2019).

We quantified the percentage of each phenotype under control conditions and PQ exposure (75 μg/mL for 48 h) (Supplementary Table 1). We observed distinct changes in vacuolar morphology across the four yeast strains. Specifically, phenotype A prevalence significantly decreased in NA (64 % control vs. 13 % PQ; p-value = 0.002, Kruskal

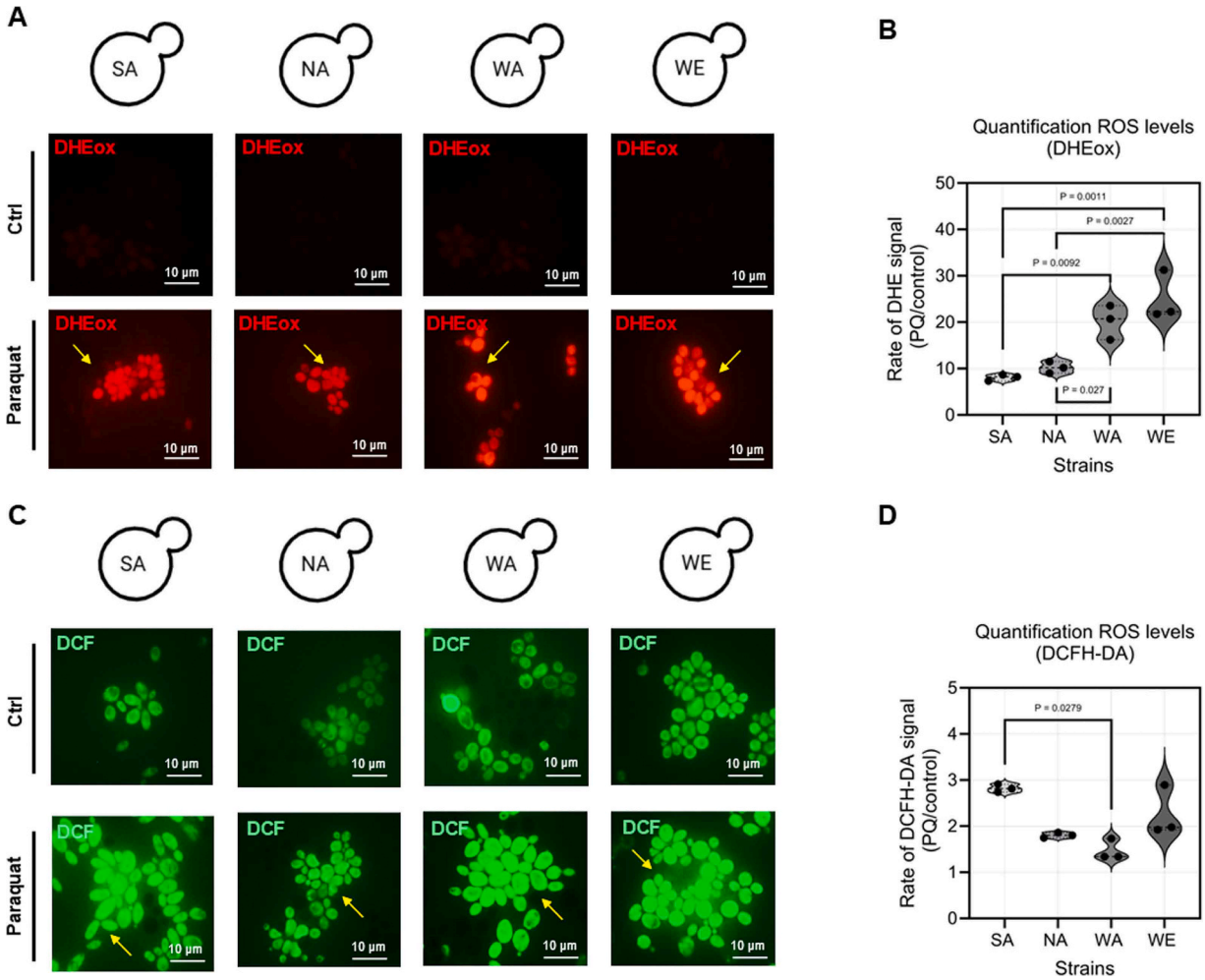

Fig. 2. Cellular response of *S. cerevisiae* to oxidative stress (superoxide anion) induced by PQ exposure. (A) Confocal images of DHE staining in untreated and PQ-exposed (75 μg/mL) SA, NA, WA, and WE yeast strains, captured at 63x magnification with 5x zoom. Yellow arrows indicate red fluorescence, marking oxidized DHE probe (DHE_{ox}) by reactive molecules. (B) Average fold change (PQ/control) in ROS (DHE) levels across strains, quantified from confocal micrographs. (C) Confocal images of DCFD-DA staining in untreated and PQ-exposed SA, NA, WA, and WE strains, visualized at 63x magnification with 5x zoom. Yellow arrows highlight green fluorescence in all strains exposed to PQ. (D) Average fold change (PQ/control) in ROS (DCF) levels from confocal micrograph quantification. Biological replicates (N = 3). Data are presented as mean ± SE. Statistical tests: Shapiro-Wilk for normality (p-value > 0.05), ANOVA test p-value < 0.05, post-hoc Tukey. Statistical significance indicated by asterisks: p-value ≤ 0.05 (*), p-value < 0.01 (**), p-value < 0.001 (***), p-value < 0.0001 (****), ns = not significant (p-value > 0.05). Statistical analysis was performed using SPSS v20.0 and plotted using GraphPad.

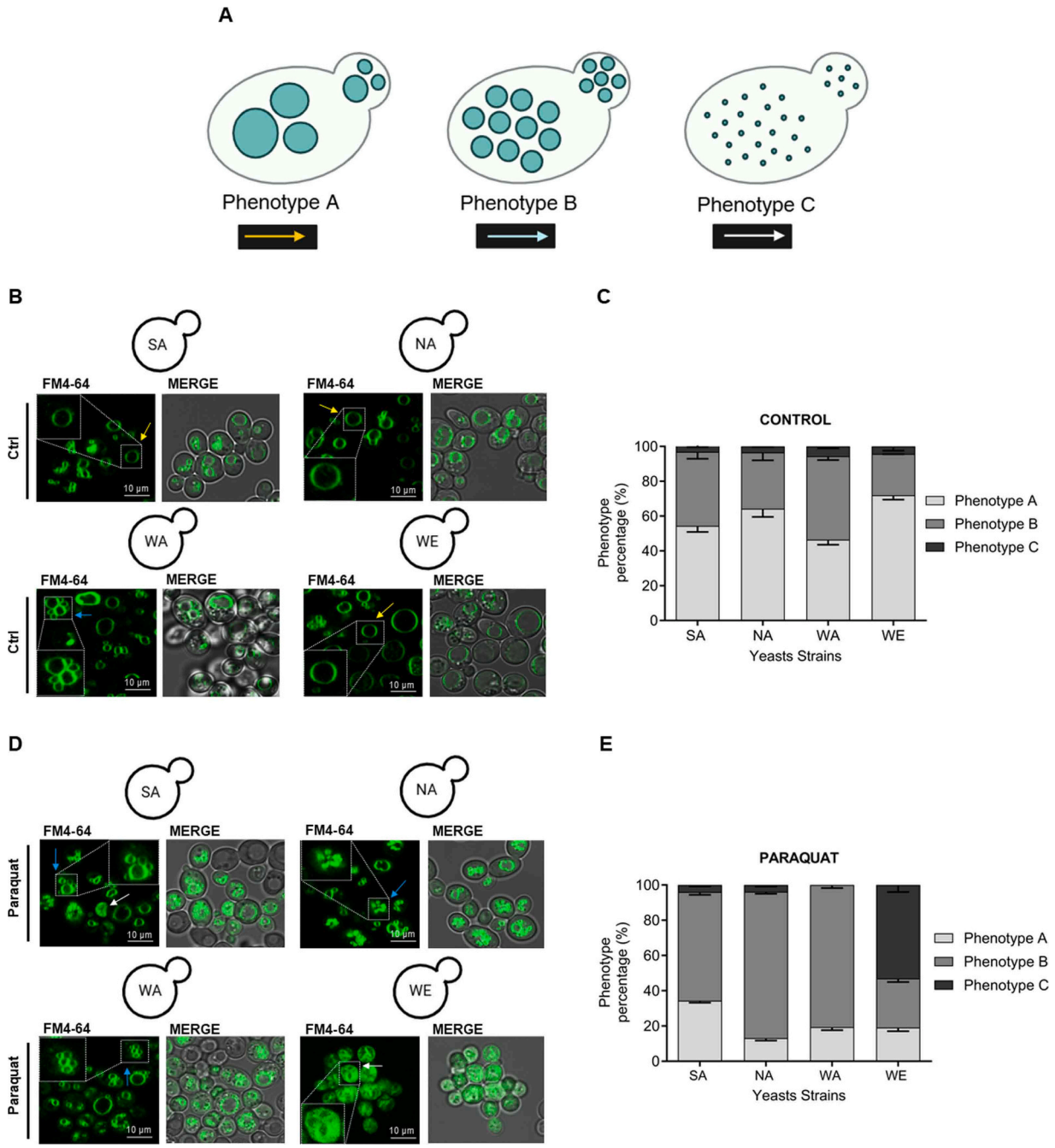

Fig. 3. Cellular response of *S. cerevisiae* to PQ-exposure involving vacuolar changes. (A) Diagram of vacuolar morphologies categorized into phenotypes A, B, and C. (B) Confocal microscopy images of FM4–64 staining in SA, NA, WA, and WE yeast strains under control conditions. (C) Quantification of vacuolar phenotypes under control conditions. (D) Confocal microscopy images of FM4–64 staining in SA, NA, WA, and WE yeast strains under PQ treatment. (E) Quantification of vacuolar phenotypes under PQ treatment. Yellow arrows indicate phenotype A, blue arrows indicate phenotype B, and white arrows indicate phenotype C. Biological replicates (N = 3). Data are presented as mean ± SD. Statistical tests: Shapiro-Wilk for normality (p-value > 0.05), Kruskal-Wallis test p-value < 0.05. Statistical significance indicated by asterisks: p-value ≤ 0.05 (*), p-value < 0.01 (**), p-value < 0.001 (***), p-value < 0.0001 (****), ns = not significant (p-value > 0.05). Statistical analysis was performed using SPSS v20.0 and plotted using GraphPad.

Wallis) and WE (79 % control vs. 19 % PQ; p-value = 0.006, Kruskal Wallis) when comparing the control condition (Figs. 3B, 3C) to PQ treatment (Figs. 3D, 3E). In contrast, no significant differences were found for phenotype A in SA (p-value = 0.273, Kruskal Wallis) and WA (p-value = 0.184, Kruskal Wallis).

Surprisingly, a significant increase in phenotype B, characterized by multiple small vacuoles (51 % increase), was observed exclusively in strain NA (32 % control to 83 % PQ; p-value = 0.009, Kruskal Wallis) (Figs. 3C, 3E). In contrast, phenotype C, characterized by highly fragmented vacuoles, decreased significantly only in strain WA (33 % increase; 6 % control vs. 0 % PQ; p-value = 0.016, Kruskal Wallis) (Figs. 3C, 3E). Micrographs (Figs. 3B, 3D) support these findings, showing a clear decrease in phenotype A and a corresponding increase in phenotype B in PQ-treated WA strain (Fig. 3E) compared to the control (Fig. 3C).

Intriguingly, the WE strain exhibited a striking increase in phenotype C, rising from 4 % in the control condition (Fig. 3D) to 53 % in PQ-exposure cells (Fig. 3E) (p-value = 0.082, Kruskal Wallis). While this

change did not reach statistical significance, a shift in vacuolar morphology is observed (Figs. 3B and 3D). Compared to the control condition, the PQ-treated WE strain displays a marked decrease in phenotype A and a dramatic increase in phenotype C. This transition towards a fragmented vacuolar state (phenotype C) in WE upon PQ exposure may represent a stress response mechanism to preserve organelle integrity for survival.

2.4. Superoxide levels correlate with physiological growth across PQ-treated yeast strains

To elucidate the compensatory mechanism to PQ exposure, we examined the relationships between the different measured traits through correlations. Multiple correlations were performed between PQ-induced fold change in μMax, DHE and DCFH-DA probes, and vacuolar morphologies A, B and C. Most traits were not interconnected (Pearson correlations) (Supplementary Table 2). However, a significant negative correlation (Pearson correlation: r = -0.97, p-value = 0.032) emerged between changes in superoxide anion levels and reproductive fitness (Figs. 4A and 4B), suggesting a shared adaptive response to PQ exposure involving intracellular ROS levels and the ability of yeasts to reproduce.

2.5. Genetic determinants of phenotypic responses to PQ exposure

We selected SA, NA, WA, and WE strains for this study because their genomes are fully sequenced (Liti et al., 2009), facilitating the association of gene variants with phenotypes. Considering the established roles of genes involved in lysosomal function and PD development, including humans exposed to pesticides (Ngo et al., 2024), we investigated genomic variations in this pathway across the four yeast strains. We analyzed 41 lysosomal/vacuolar genes, of which only 28 had orthologs in yeast. In these 28 vacuolar genes, we identified a total of 954 predicted variants, comprising 23.7 % nonsynonymous, 76.1 % synonymous, 0.1 % frameshift deletion, and 0.1 % start-loss variants (Supplementary Table 3). We hypothesized that missense variants, which are likely to impact protein function, could contribute to PQ responses. To explore this, we performed Pearson's correlations between the number of deleterious variants as predicted by SIFT (Sorting Intolerant From Tolerant) in vacuolar genes with multiple phenotypes: μMax, DHE (superoxide levels), and vacuolar phenotypes across four yeast strains. Only the statistically significant associations were listed in Table 1.

The number of *YEH1* variants showed a significant negative correlation with μMax (Pearson's r = -0.980, p-value = 0.020). A significant positive correlation was found between *SSA2* variant count and DHE-measured ROS levels (r = 0.972, p-value = 0.028). Phenotype B was positively correlated with variants in *FEN2*, while an unexpected negative correlation was observed with variants in *YHC3* (Table 1). However, after adjusting for multiple comparisons (see "Experimental procedures"), these correlations did not remain significant when considering all nonsynonymous and synonymous variants within the gene set. This loss of significance was likely due to the conservative nature of the Bonferroni correction. Consequently, we decided to functionally validate one of the identified genes.

2.6. fen2-deletion increases vacuolar fragmentation upon PQ exposure

FEN2 is a proton-pantothenate symporter, and its human ortholog, SLC17A5, is a lysosomal protein associated with sialic acid storage disorder and considered a potential susceptibility factor for PD. Given the strong correlation observed between the number of *FEN2* variants and the percentage of vacuolar B phenotype, we investigated the effect of *FEN2* deletion on PQ-induced vacuolar disaggregation. Vacuolar morphology was classified into phenotypes A, B, and C in both the wild-type (BY4742 strain) and the *Δfen2* strain under control (Figs. 5A, 5B) and following PQ exposure (200 μg/mL for 48 h) (Figs. 5C, 5D). The percentage of each phenotype was quantified (Figs. 5B, 5D and Supplementary Table 4). Under control conditions, the *Δfen2*, showed a significant increase in the percentage of phenotype B (p-value = 0.0313, T-test) and C (p-value = 0.0204, T-test), along with a decrease in the percentage of phenotype A (p-value = 0.0114, T-test) compared to BY4742 (Fig. 5B). Notably, the decrease in phenotype A of Δfen2 was amplified upon PQ exposure (p-value = 0.0478, T-test). In addition, we

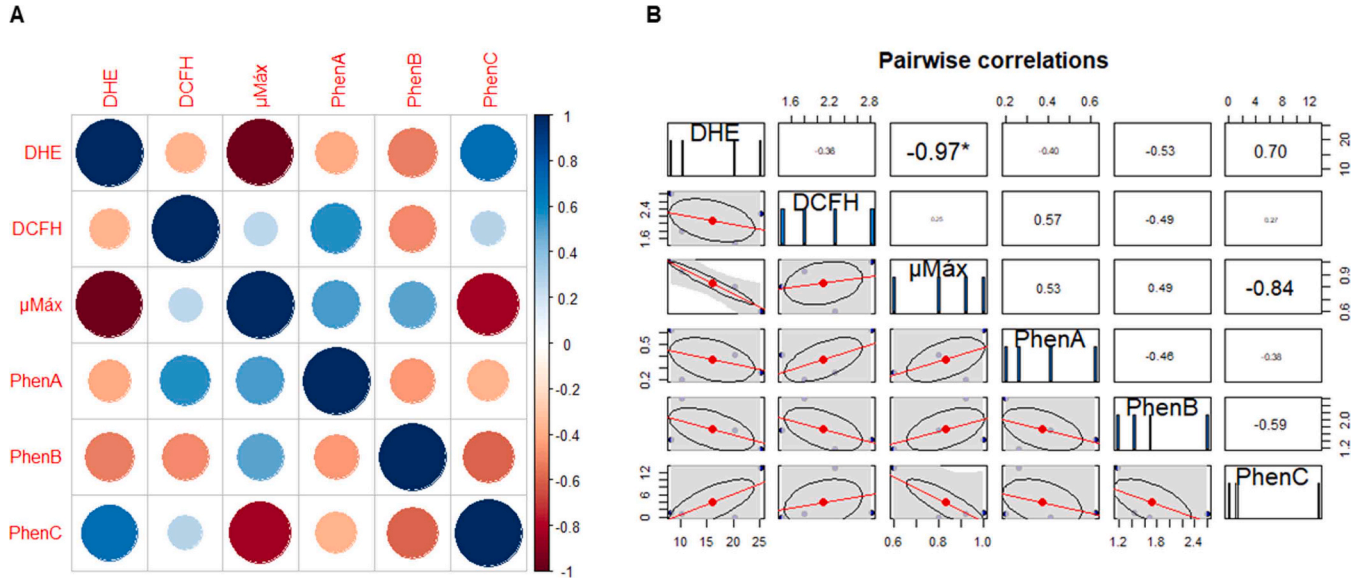

Fig. 4. Interplay between physiological parameters, oxidative stress, and vacuolar morphology. (A) Plot showing multiple correlations between fold change in μMax, DHE probe, DCFH-DA probe, and phenotypes A, B, and C. (B) Pairwise correlations between fold change in μMax, DHE probe, DCFH-DA probe, and vacuolar phenotypes A, B, and C. Biological replicates (N = 4). Data are presented as mean ± SE. Statistical tests: Pearson correlation p-value < 0.05 in μMax, DHE probe, DCFH-DA probe, phenotype A and phenotype B. For phenotype C and combinations with other parameters, Spearman correlation was applied. Normality was tested using Shapiro-Wilk (p-value > 0.05). Statistical significance indicated by asterisks: p-value ≤ 0.05 (*), p-value < 0.01 (**), p-value < 0.001 (***), p-value < 0.0001 (****), ns = not significant (p-value > 0.05). Statistical analysis was performed using SPSS v20.0 and plotted using GraphPad.

Table 1
Correlations of lysosomal and oxidative stress genes with the number of variants in yeast strains. The potential effects of variants in each gene of the four yeast strains were determined using SIFT software. The number of variants in oxidative stress and lysosomal genes was correlated with μMáx, ROS levels (DHE probe), and phenotype B using Pearson correlations. To adjust for multiple comparisons, we applied the Bonferroni procedure to control for the error rate and establish a corrected statistical significance threshold and adjusted P-value (P_{adj} *a*) based on a significance level of 0.05. Statistical analysis was performed and plotted using RStudio v4.3.1.

		Number of variants				μMax			DHE			Phenotype B		
Human lysosomal genes	Orthologue in *S. cerevisiae*	SA	NA	WA	WE	*P-value*	P_{adj} *a*	*r*	*P-value*	P_{adj} *a*	*r*	*P-value*	P_{adj} *a*	*r*
CLN3	*YHC3*	5	4	3	9	0.438	1.000	−0.562	0.489	1.000	0.511	**0.025**	0.300	**−0.975**
LIPA	*YEH1*	0	3	6	11	**0.020**	0.240	**−0.980**	0.745	1.000	−0.256	0.368	1.000	−0.633
SLC17A5	*FEN2*	6	7	8	1	0.398	1.000	0.601	0.528	1.000	−0.472	**0.026**	0.312	**0.974**
ABHD5	*ICT1*	8	10	12	3	0.540	1.000	0.460	0.400	1.000	−0.600	**0.032**	0.384	**0.968**
ATG5	*ATG5*	6	7	6	3	0.197	1.000	0.803	0.659	1.000	−0.341	**0.048**	0.576	**0.952**
HSPA8	*SSA2*	32	27	27	31	0.965	1.000	0.035	**0.028**	0.336	**0.972**	0.255	1.000	−0.745
		87	96	91	65	0.273	1.000	0.727	0.565	1.000	−0.436	**0.018**	0.216	**0.982**
PQ: μMáx (OD/h)		**0.26**	**0.24**	**0.18**	**0.14**									
PQ: DHE (A.F.U)		**23668**	**15665**	**17878**	**25999**									
PQ: Phenotype B (%)		**61.7**	**83.0**	**80.6**	**27.8**									

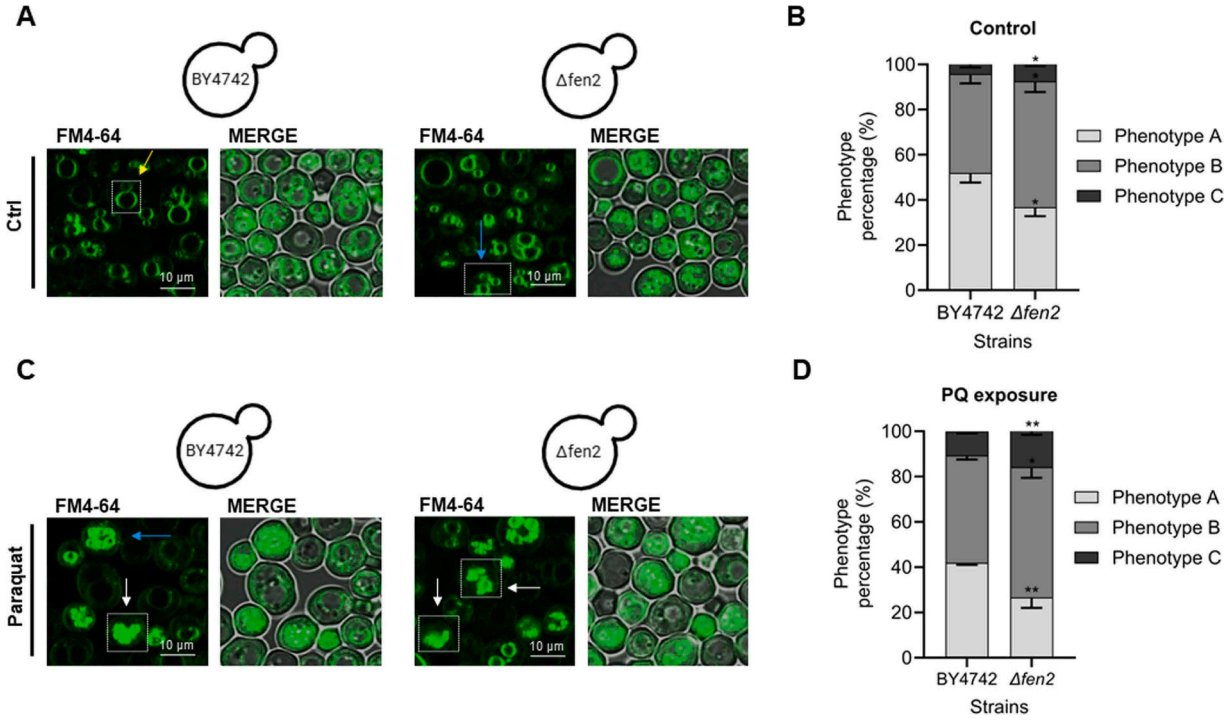

Fig. 5. Vacuolar response of BY4742 (ref) and the *fen2*-deletant strain to PQ exposure. (A) Confocal microscopy of FM4–64 staining in BY4742 and *fen2*-deletant (*Δfen2*) control condition. (B) Quantification of vacuolar phenotypes in the control condition. (C) Confocal microscopy of FM4–64 staining in BY4742 and *Δfen2* under PQ treatment (200 μg/mL). (D) Quantification of vacuolar phenotypes under PQ treatment. Yellow arrows: phenotype A, blue arrows: phenotype B, and white arrows: phenotype C. Biological replicates (N = 3–6). Data are presented as mean ± SD. Statistical tests: Shapiro-Wilk for normality (p-value > 0.05), T-test p-value < 0.05. Statistical significance indicated by asterisks: p-value ≤ 0.05 (*), p-value < 0.01 (**), p-value < 0.001 (***), p-value < 0.0001 (****), ns = not significant (p-value > 0.05). Statistical analysis was performed using SPSS v20.0 and plotted using GraphPad.

found an increased effect of PQ on phenotype C of Δfen2 (p-value = 0.0040, T-test). Specifically, PQ-treated *Δfen2* strain exhibited a more pronounced increase in the percentage of phenotype B (p-value = 0.0270, *t*-test) and C (p-value = 0.0071, *t*-test), and a more pronounced decrease in the percentage of phenotype A (p = 0.0051, *t*-test) compared to BY4742 (Fig. 5D). These findings suggest a potential role for FEN2 in mediating the vacuolar response to PQ.

2.7. fen2-deletion decreases cell growth and increases oxidative stress markers upon PQ exposure

Following the validation of the role of FEN2 in vacuolar disaggregation upon PQ exposure, a more comprehensive understanding of its participation was sought. Initially, growth rates were analyzed because they integrate all the molecular processes within a cell. The *fen2Δ* strain replicated slower than the wild-type strain under control conditions, and this effect was exacerbated when exposed to PQ (Fig. 6A). This difference was further evidenced by quantifications of both the Area Under the Curve (AUC) (Fig. 6B; p = 0.0003, ANOVA) and fold change in μMax (Fig. 6C; p = 0.0288, T-test). These results suggest that FEN2 deletion is associated with enhanced cellular stress under PQ exposure.

Consequently, ROS levels were measured in the *Δfen2* and BY4742 strains using DCFH-DA and DHE probes. Significant increases in the DCFH-DA signal were quantified following PQ exposure in both *Δfen2* (p < 0.0001, ANOVA) and BY4742 (p < 0.0001, ANOVA) (Fig. 6D). Then, we calculated the fold-change in DCFH-DA fluorescence in PQ-

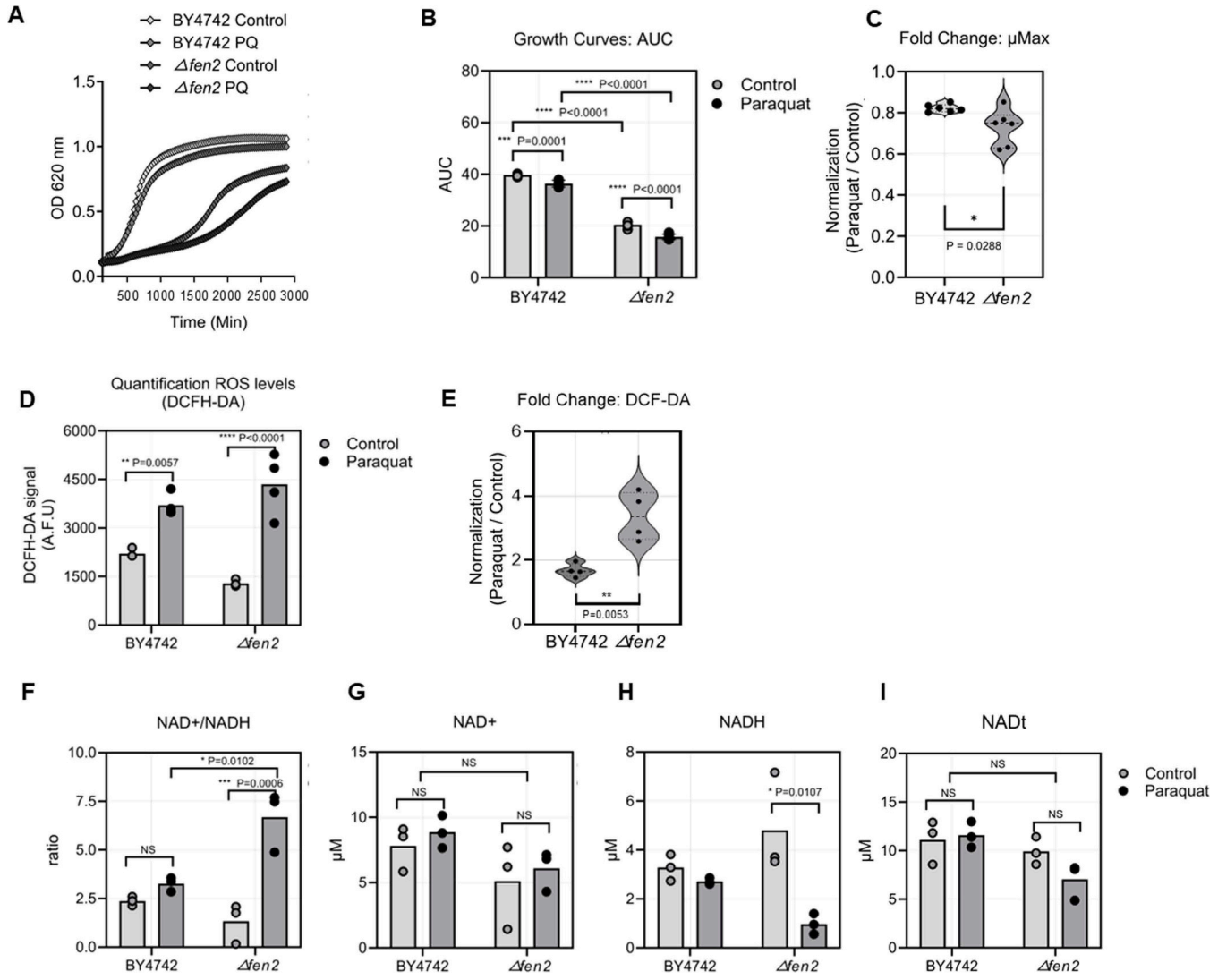

Fig. 6. Growth and oxidative response of BY4742 (ref) and *fen2*-deletant strain to PQ (A) Growth curves, (B) AUC, and (C) μMax in BY4742 and *Δfen2* under PQ treatment (200 μg/mL) and control. (D) DCFH-DA levels μMax in BY4742 and *Δfen2* under PQ treatment (200 μg/mL) and control. (E) Quantification of DCFH-DA levels, expressed as fold-change, by genotype. (F-I) Measurements of NAD+ /NADH ratio, NAD^+, NADH, and NADt in BY4742 and *Δfen2* under PQ treatment (200 μg/mL) and control. Biological replicates (N = 3–4). Data are presented as mean ± SD. Statistical tests: Shapiro-Wilk for normality (p-value > 0.05), T-test p-value < 0.05. Statistical significance indicated by asterisks: p-value ≤ 0.05 (*), p-value < 0.01 (**), p-value < 0.001 (***), p-value < 0.0001 (****), ns = not significant (p-value > 0.05). Statistical analysis was performed using SPSS v20.0 and plotted using GraphPad.

treated cells by genotype. We found a 1.7 increase in the control cells, compared to a 3.4-fold increment in *Δfen2* (p = 0.0053, T test, Fig. 6E). In contrast, no differences were found in the DHE signal in the *Δfen2* strain between control and PQ treatment (data not shown). This outcome suggests a specific shift in ROS metabolism where FEN2 deletion promotes hydrogen peroxide formation instead of superoxide radicals.

To further characterize the associated redox imbalance, the oxidized and reduced forms of nicotinamide adenine dinucleotide (NAD^+ and NADH) were measured with the NAD+ /NADH ratio being used as an indicator of mitochondrial function (Fig. 6F-I). While no significant differences were found between *Δfen2* and BY4742 in control or PQ exposure conditions for NAD^+ or total NAD (NADt) levels (Fig. 5G), NADH levels in the *Δfen2* strain significantly decreased under PQ exposure compared to the control condition (p = 0.0107, ANOVA).

Importantly, the NAD+ /NADH ratio was significantly elevated in the *Δfen2* strain treated with PQ compared to the control (p = 0.0006, ANOVA) (Fig. 6E). Upon comparison with BY4742, the Δfen2 strain exhibited a significantly higher NAD+ /NADH ratio after PQ exposure (p = 0.0102, ANOVA) (Fig. 5G). This observed increase is likely attributable to the NADH-consuming process of PQ reduction, representing a compensatory response of the *Δfen2* strain to mitigate PQ-induced stress.

3. Discussion

In humans, PQ is highly toxic, with potential absorption through the gastrointestinal tract, skin contact, or inhalation. Exposure can induce several pathologies, including lung fibrosis, liver tumors, and PD (Donaher and Van den Hurk, 2023). PQ disrupts the intracellular redox cycle, leading to mitochondrial fragmentation via the generation of ROS and reactive nitrogen species, as well as lysosomal damage (Pascua-Maestro et al., 2017). These cellular injuries can trigger apoptosis in dopaminergic neurons, contributing to PD pathogenesis (See et al., 2022). Given that these pathways are conserved in eukaryotes, *S. cerevisiae* has been a valuable model for elucidating PQ toxicity mechanisms (Sillapawattana et al., 2024). However, the majority of these investigations have focused on single yeast strains, thereby limiting our understanding of how genetic diversity influences the

cellular and molecular adaptive strategies to PQ.

Our study demonstrates a differential impact of PQ on μMax across four genetically diverse *S. cerevisiae* strains. This differential response is driven by genomic variation, shaped by distinct evolutionary histories and ecological adaptations. Under physiological conditions, μMax is controlled by *GCN4*, a transcriptional factor that regulates amino acid biosynthesis, along with other factors such as *FIL1* and *GCN2* (Duncan et al., 2018; Fendt et al., 2010). Further investigation is required to determine whether changes in amino acid homeostasis relate to the strain-specific variations in μMax upon PQ exposure. Crucially, our results highlight the significance of genetic background in determining yeast susceptibility to PQ toxicity, which is consistent with previous findings in other models (Lovejoy et al., 2021).

Oxidative damage is a PD hallmark. Notably, a correlation exists between oxidative stress markers and PD age of onset and severity in both blood and cerebrospinal fluid (Takahashi et al., 2021). Consistent with these observations, our findings indicate that strains exhibiting high superoxide levels show significantly reduced reproductive fitness (a susceptibility phenotype), implying less efficient mechanisms for mitigating oxidative stress. Accordingly, this finding highlights the value of yeast with diverse genetic backgrounds for precision medicine studies and suggests that strategies aimed at reducing oxidative damage could be useful to prevent PQ-induced cell damage in humans.

Superoxide is a common product of electron leakage from donor redox centers within the mitochondrial electron transport chain. This radical species subsequently leads to the formation of secondary products such as peroxide, a reaction catalyzed by mitochondrial superoxide dismutase. Unexpectedly, our results revealed no significant correlations between peroxide levels and any of the parameters measured, which suggests that superoxide dismutase activity varies across the yeast strains. In the PQ-treated cells, superoxide may directly damage lipids, proteins, and DNA or exert its effects in combination with other radical species, including peroxynitrite (Naspolini et al., 2021).

In yeast, vacuoles, the functional counterparts of mammalian lysosomes, are highly dynamic organelles that exhibit a continuous cycle of fusion and fission in response to environmental cues (Aufschnaiter and Büttner, 2019). Significantly, oxidative stress is a recognized inducer of vacuolar fragmentation (Kim et al., 2021). This process is under the stringent control of Vacuolar Protein Sorting 1 (VPS1) and Autophagy-Related Protein 8 (ATG8) (Mikawa et al., 2010). VPS1, a protein implicated in intracellular trafficking, is also essential for the development of cellular resistance to oxidative insults. Concurrently, Atg8 contributes to the structural integrity of the vacuolar membrane, independent of its canonical role in autophagy. Furthermore, double mutants in VPS1 and ATG8 exhibit greater sensitivity to PQ, osmotic stress, and calcium overload compared to the single mutations, indicating impaired vacuolar function (Mikawa et al., 2010). Therefore, further investigation is required to elucidate the specific role of these proteins in determining the spectrum of PQ susceptibility observed across diverse yeast strains.

Genetic studies demonstrate a direct association between various mitochondrial and lysosomal genes and the risk of idiopathic PD (iPD) (Blauwendraat et al., 2020). A key example is the *GBA1* gene, which encodes for lysosomal β-glucocerebrosidase (GCase). *GBA1* variants are a major genetic risk factor for PD development. Remarkably, GCase plays dual roles: in the lysosome, it degrades glucosylceramide, and in mitochondria, it promotes complex I stability (Klein and Outeiro, 2023). Given that pesticides target mitochondria, a recent study identified an enrichment in genomic variants in 26 genes associated with lysosomal function. These findings support the idea that impaired lysosomal and mitochondrial dysfunction is necessary for PD to develop (Ngo et al., 2024). Similarly, our yeast study shows significant correlations between the number of missense variants in different genes associated with vacuolar/lysosomal function and PQ-induced phenotypes. Our analysis revealed a positive association between an increased number of variants in the *FEN2* gene with a rise in phenotype B. In yeast, *FEN2* is known to coregulate carbon and nitrogen catabolism, amino acids, and ergosterol biosynthesis (Marcireau et al., 1996). The human orthologue of this gene belongs to the *SLC17A* transport family and is implicated in sialuria, a sialic acid lysosomal storage disorder with enlarged lysosomes (Huizing et al., 2021). While an exome sequencing study in 2017 identified *SLC17A5* as a potential PD susceptibility gene (Robak et al., 2017), a 2025 study focused on European ancestry found no association between *SLC17A5* common variants and PD risk (Sabir et al., 2025). This discrepancy highlights the need for comprehensive genetic analyses across diverse populations, as employed in our yeast study, to fully understand the role of sialic acid homeostasis in different PD subtypes associated with lysosomal dysfunction. Functionally, our results showed a significantly increased vacuolar fragmentation in a *fen2*-deletant strain, likely due to the accumulation of a sialic acid-like product in yeast. This may reflect the sialuria phenotype in humans, where lysosomal dysfunction from transport deficiency leads to similar lysosomal fragmentation and could be implicated in pesticide-induced PD.

The lack of FEN2 significantly altered the cellular redox state upon PQ exposure, suggesting that mitochondrial function is compromised in addition to the observed vacuolar defects. This impairment could occur either i) directly via vacuole-mitochondrial contact sites or ii) indirectly through lysosomal/autophagy dysfunction caused by the buildup of partially degraded material in the vacuole, a mechanism similar to that observed in *GBA1*-related PD (Rubilar et al., 2024). Furthermore, the observed shift from increased superoxide to peroxide radicals suggests the activation of SOD1, the enzyme that catalyzes this conversion. This interpretation is consistent with a recent report describing that SOD1 can be recruited to lysosomes to maintain their activity and integrity (Zheng et al., 2025). Collectively, these observations suggest that the increase in peroxide levels in the *Δfen2* strain upon PQ exposure may be occurring in both mitochondria and vacuoles.

Cells possess mechanisms to counteract oxidative stress, including the regulation of the balance between oxidized and reduced nicotinamide adenine dinucleotide forms, a process particularly relevant for brain diseases (Lautrup et al., 2019). Our experiments revealed a significant increase in the NAD^+/NADH ratio in the *Δfen2* strain following PQ exposure. This elevation is likely due to the NADH-consuming process of PQ reduction and represents a compensatory response to mitigate PQ-induced stress, similar to responses described in dopaminergic neurons exposed to PQ (Lei et al., 2014). PQ-induced redox imbalance can also affect downstream pathways, such as lipid peroxidation, ultimately leading to neuronal toxicity (Naspolini et al., 2021). Maintaining balanced NAD^+/NADH ratio is essential for mitigating oxidative stress and supporting neuronal metabolism, thus offering potential strategies to protect against neurodegenerative diseases like PD (Curtis et al., 2022). Consequently, understanding these molecular redox changes in yeast could provide valuable insights into the mechanisms of PQ toxicity and PD pathogenesis.

Our study also has limitations: i) the use of a small number of strains; which limits the power to identify significant associations across traits; ii) the focus on only on two PD-related phenotypes: ROS and vacuolar adaptations, omitting others like proteostasis; iii) the use of domesticated yeast strains, while offering genetic stability, may not fully represent the genetic and phenotypic variability found in wild populations; and iv) the phenotypic characterization lacked detailed mechanistic assays. However, by investigating the cellular and molecular responses underlying resistance and susceptibility to PQ across these diverse genetic backgrounds, our study reveals the biological foundation supporting these differences and highlights the fundamental role of genetics in understanding these complex processes.

In conclusion, our work explores the cellular and molecular mechanisms underlying PQ toxicity in four distinct yeast backgrounds, demonstrating their utility as effective proxies for studying PQ susceptibility and resistance in humans. Furthermore, we validated the inverse association between superoxide levels and reproductive fitness, and confirmed the role of *FEN2* in PQ-induced vacuolar disaggregation.

Understanding the biology of the PQ-resistant strains may facilitate the design of strategies to prevent pesticide-induced PD. Future work should leverage gene mapping studies and omics in *S. cerevisiae*, followed by rigorous validation in animal models and human cells.

4. Experimental procedures

4.1. Yeast strains and culture conditions

The four haploid (*MAT α* and *MAT a*) *S. cerevisiae* strains used in this study were: North American (NA; YPS128, *MAT α/a, ho: HygMX, ura3::kanMX*), West African (WA; DBVPG6044, *MAT α/a, ho: HygMX, ura3::kanMX*), Sake (SA; Y12, *MAT α/a, ho: HygMX, ura3::kanMX*) and. Wine/European (WE; DBVPG6765, *MAT α/a, ho: HygMX, ura3::kanMX*) (Brice et al., 2018; Salinas et al., 2016). These strains were stored in solid media (YPD) at 4°C. Liquid and solid culture media were used depending on the experiments to be performed: YPD media (2 % glucose, 2 % peptone, 1 % yeast extract) and YNB (0.67 % YNB base without amino acids, 0.2 % uracil, 0.0875 % com drop out and 2 % glucose). Validation studies were performed using the BY4742 strain, specifically the wild-type (WT; Accession Y10000), the *fen2*-deletant (BY4742; MATα; his3Δ1; leu2Δ0; lys2Δ0; ura3Δ0; YCR028c::kanMX4). Reference and deletant strain were obtained from Euroscarf (http://www.euroscarf.de).

4.2. Growth curves conditions

Yeast cells were pre-cultured in 200 µL of YNB medium supplemented with uracil (0.2 % uracil) for 48 h at 28 °C. For the experimental run, the four yeast strains were inoculated to an optical density (OD) of 0.03–0.1 (wavelength of 620 nm) in 200 µL of medium and incubated without shaking at 28 °C for 48 h (YNB control and Paraquat dichloride hydrate (CAS No. 75365–73–0, Sigma Aldrich-Merck, Germany) was prepared as a stock solution at a concentration of 10 mg/mL in sterile distilled water, owing to its high solubility. This stock solution was subsequently utilized for all herbicide exposure experiments at 75 µg/mL) in a Tecan Sunrise absorbance microplate reader (Tecan Trading AG, Männedorf, Switzerland). OD was measured every 30 min using a 620 nm filter. Each experiment was performed in triplicate. Growth rates for each strain were calculated as previously described (García-Ríos et al., 2014; Quispe et al., 2017). Briefly, OD measurements as a function of time were fitted to the mathematical model of the re-parameterized Gompertz sigmoid curve describing microbiological temporal growth, previously proposed (Zwietering et al., 1990) from which growth rates were obtained. The parameters of each curve were processed in the GrowthRates software to obtain OD max, µmax, and the average time of the lag phase. Finally, the area under the curve (AUC) values of the growth curves were calculated using R commands.

4.3. Measurement of levels of reactive oxygen species (ROS)

The yeast strain cultures were incubated for 48 h at 28°C in 3 mL of YNB medium and centrifuged at 1700 x g at 4 °C for 4 min. Intracellular levels of superoxide anion were detected through the dihydroethidium (DHE) probe (Thermofisher Scientific, NºD1168, U.S.A), and intracellular levels of hydrogen peroxide (H_2O_2) were detected through the 2′,7′-dichlorofluorescein diacetate (DCFH-DA) probe (Sigma Aldrich, NºD6883, U.S.A). The pellet was incubated with the DHE probe at a concentration of 10 µg/mL (Mendes-Ferreira et al., 2010) in 500 µL of PBS (80 mM Na_2HPO_4, 20 mM NaH_2PO_4 and 100 mM NaCl) (Rego et al., 2020) for 30 min and washed with PBS as previously reported (Mendes-Ferreira et al., 2010; Rego et al., 2020). The DCFH-DA probe was used at a concentration of 10 µM (Chapela et al., 2022) in 500 µL of PBS for 1 h and washed with a PBS buffer. Fluorescence intensity was visualized using a Leica SP8 confocal microscope (Leica Microsystems, Germany) at 518/605 nm for DHE and 490/530 for DCFH-DA. For microscopic analysis, 4 µL of each incubated strain (DHE and DCFH-DA probe) were taken, added to a slide, and squeezed with a coverslip gently for *in vivo* visualization and observed under a microscope using a 63X objective and 5X magnification. Images were processed in ImageJ (Schneider et al., 2012) and LASX software (Leica Microsystems, Germany).

4.4. FM4-64 internalization assay in S. cerevisiae: vacuolar phenotypes

Yeasts were seeded on a plate with YPD medium and 2 % agar-agar. Isolations were made from each strain to obtain single colonies previously incubated at 28°C without shaking for 48 h. Then, inocula were transferred into 500 µL of liquid YPD and incubated with 3 µM of FM4–64 (Ex: 565 nm - Em: 744 nm) (ThermoFisher Scientific, N° F34653, U.S.A) for 24 h in 48-hour cultures in control condition (Seeley et al., 2002) and with 75 µg/mL Paraquat at 28°C with shaking (150 rpm) in the dark. 4 µL of each incubated strain was added to a slide and squeezed with a coverslip gently for in vivo viewing and observed on Leica SP8 confocal microscope (Leica Microsystems, Germany), using 63X objective and 5X magnification. Images were processed in ImageJ and LASX software (Leica Microsystems, Germany). The vacuolar characteristics of 110–150 cells per field were analyzed and classified according to their phenotype into "A", "B" or "C", as proposed by Seeley E. et al. (Seeley et al., 2002). The assay was repeated three times and quantified by three researchers independently for each yeast strain.

4.5. Measurement of intracellular NAD+ and NADH levels

Intracellular NAD+ and NADH levels and NAD+ /NADH ratio were determined by NAD+ /NADH Assay Kit (Abcam, Cat #65348, Cambridge, UK) according to the manufacturer's instructions, with modifications. Briefly, 2 mL of yeast culture per condition was harvested, washed with ice-cold PBS, and lysed using 300 µL of extraction buffer through three cycles of freezing (liquid nitrogen), vortexing, and thawing. The lysate was centrifuged at 10,000 g for 10 min at 4°C to remove proteins. Then, half of the supernatant volume was incubated at 60 °C for 30 min to decompose NAD+ , while the other half volume was designated as total NAD (NADH plus NAD^+). Then, 0.85 µL of each half of the supernatant was then transferred to a clear-bottom 386-well plate. For each assay a series of NADH standards of 0, 0.4, 0.8, 1.2, 1.6, and 2 µM per well was included. 33.3 µL of NAD cycling buffer and enzyme mix (32.97 µL cycling buffer and 0.33 µL cycling enzyme mix from the manufacturer) was added to each sample and incubated for 5 min at room temperature to convert all NAD+ to NADH. 1.7 µL of the manufacturer's NADH developer was added to each well. Absorbance at 450 nm was measured using a plate reader after 1 h of incubation. Total NADt and NADH levels were calculated using a standard curve and expressed as µM.

4.6. Statistical analysis

Growth parameters µMax, ROS level by DHE and DCFH-DA, NAD+ / NADH levels, and percentage of vacuolar phenotypes were used as quantitative variables in the control condition and PQ at a 75 µg/mL concentration. For reference and deletant strain, we used a PQ concentration at 200 µg/mL. Shapiro-Wilk normality test $p > 0.05$, parametric ANOVA test $p < 0.05$ with multiple comparisons, and non-parametric Kruskal-Wallis test p-value < 0.05 with multiple comparisons were used for all measurements. For the percentage of vacuolar phenotypes in deletant strains validation, the Shapiro-Wilk normality test ($p > 0.05$) and T-test ($p < 0.05$) were done. Sample "N" in the experiments was 5 biological replicates and 3 technical replicates per sample for µMax, 6 biological replicates and 3 technical replicates per sample for ROS level by DHE and DCFH-DA probe, and 3 biological replicates with 3 technical replicates per sample for quantification of vacuolar phenotypes, 6 biological replicates and 3 technical replicates

per sample for μMax in Δfen2 and BY4742 strains, 3 biological replicates and 3 technical replicates per sample for NAD+ /NADH in Δfen2 and BY4742 strains and 4 biological replicates and 3 technical replicates per sample for DHE and DCFH-DA in Δfen2 and BY4742 strains. Statistical significance was considered for a value of $p < 0.05$. Furthermore, multiple correlations were conducted in this study. Pearson correlations were performed for the fold change of DHE, DCFH, μMax, and vacuolar phenotypes A, B, and C, as the data exhibited normal distribution (Shapiro-Wilk test $p > 0.05$). The potential effects of variants in each gene of the four yeast strains were determined using SIFT software (Supplementary Table 3) and the *S. cerevisiae* S288C reference genome (https://www.yeastgenome.org/). The number of variants in oxidative stress and lysosomal genes was correlated with μMáx, ROS levels (DHE probe), and phenotype B using Pearson correlations. To adjust for multiple comparisons, we applied the Bonferroni procedure to control for the error rate and establish a corrected statistical significance threshold and adjusted P-value (P_{adj} *a*) based on a significance level of 0.05. Statistical analysis was performed in SPSS software version 20.0 (Illinois, U.S.A) and plotted in GraphPad (California, U.S.A) and RStudio (U.S.A).

CRediT authorship contribution statement

Juan Carlos Rubilar: Writing – review & editing, Writing – original draft, Methodology, Investigation, Formal analysis, Data curation, Conceptualization. **Klein Andrés D.:** Writing – review & editing, Writing – original draft, Supervision, Project administration, Methodology, Funding acquisition, Formal analysis, Data curation, Conceptualization. **Francisco A. Cubillos:** Writing – review & editing, Supervision, Methodology, Data curation, Conceptualization. **Benjamín Szenfeld:** Methodology, Formal analysis.

Declaration of Competing Interest

The authors declare that they have no known competing financial interests or personal relationships that could have appeared to influence the work reported in this paper.

Acknowledgements

This work was supported by ANID-CHILE: Fondecyt grant No 1230317 (A.D.K). The authors thank Macarena Las Heras for technical support in NAD^+ measurements.

Appendix A. Supporting information

Supplementary data associated with this article can be found in the online version at doi:10.1016/j.ecoenv.2025.119426.

Data Availability

No data was used for the research described in the article.

References

Aufschnaiter, A., Büttner, S., 2019. The vacuolar shapes of ageing: From function to morphology. Biochim. Biophys. Acta Mol. Cell Res. 1866, 957–970.
Ball, N., Teo, W.-P., Chandra, S., Chapman, J., 2019. Parkinson's disease and the environment. Front. Neurol. 10, 218.
Blauwendraat, C., Nalls, M.A., Singleton, A.B., 2020. The genetic architecture of Parkinson's disease. Lancet Neurol. 19, 170–178.
Brice, C., Cubillos, F.A., Dequin, S., Camarasa, C., Martínez, C., 2018. Adaptability of the Saccharomyces cerevisiae yeasts to wine fermentation conditions relies on their strong ability to consume nitrogen. PLoS One 13, e0192383.
Burbulla, L.F., Krüger, R., 2011. Converging environmental and genetic pathways in the pathogenesis of Parkinson's disease. J. Neurol. Sci. 306, 1–8.
Chapela, S.P., Burgos, H.I., Stella, C.A., 2022. N-Acetyl cysteine improves cellular growth in respiratory-deficient yeast. Braz. J. Microbiol 53, 791–794.
Curtis, W.M., Seeds, W.A., Mattson, M.P., Bradshaw, P.C., 2022. NADPH and mitochondrial quality control as targets for a Circadian-Based Fasting and Exercise therapy for the treatment of Parkinson's disease. Cells 11 (15), 2416.
Donaher, S.E., Van den Hurk, P., 2023. Ecotoxicology of the herbicide paraquat: effects on wildlife and knowledge gaps. Ecotoxicology 32, 1187–1199.
Duncan, C.D.S., Rodríguez-López, M., Ruis, P., Bähler, J., Mata, J., 2018. General amino acid control in fission yeast is regulated by a nonconserved transcription factor, with functions analogous to Gcn4/Atf4. Proc. Natl. Acad. Sci. U. S. A. 115, E1829–E1838.
Fendt, S.-M., Oliveira, A.P., Christen, S., Picotti, P., Dechant, R.C., Sauer, U., 2010. Unraveling condition-dependent networks of transcription factors that control metabolic pathway activity in yeast. Mol. Syst. Biol. 6, 432.
Fleming, S.M., 2017. Mechanisms of gene-environment interactions in Parkinson's disease. Curr. Environ. Health Rep. 4, 192–199.
García-Ríos, E., López-Malo, M., Guillamón, J.M., 2014. Global phenotypic and genomic comparison of two Saccharomyces cerevisiae wine strains reveals a novel role of the sulfur assimilation pathway in adaptation at low temperature fermentations. BMC Genom. 15, 1059.
Hernandez-Baixauli, J., Chomiciute, G., Tracey, H., Mora, I., Cortés-Espinar, A.J., Ávila-Román, J., Abasolo, N., Palacios-Jordan, H., Foguet-Romero, E., Suñol, D., Galofré, M., Alcaide-Hidalgo, J.M., Baselga-Escudero, L., Del Bas, J.M., Mulero, M., 2024. Exploring metabolic and gut microbiome responses to paraquat administration in male wistar rats: implications for oxidative stress. Antioxid. (Basel) 13. https://doi.org/10.3390/antiox13010067.
Huizing, M., Hackbarth, M.E., Adams, D.R., Wasserstein, M., Patterson, M.C., Walkley, S. U., Gahl, W.A., Consortium, F.S.A.S.D., 2021. Free sialic acid storage disorder: progress and promise. Neurosci. Lett. 755, 135896.
Kim, D., Song, M., Do, E., Choi, Y., Kronstad, J.W., Jung, W.H., 2021. Oxidative stress causes vacuolar fragmentation in the human fungal pathogen. J. Fungi (Basel) 7. https://doi.org/10.3390/jof7070523.
Klein, A.D., Mazzulli, J.R., 2018. Is Parkinson's disease a lysosomal disorder? Brain 141, 2255–2262.
Klein, A.D., Outeiro, T.F., 2023. Glucocerebrosidase mutations disrupt the lysosome and now the mitochondria. Nat. Commun. 14, 6383.
Lautrup, S., Sinclair, D.A., Mattson, M.P., Fang, E.F., 2019. NAD+ in brain aging and neurodegenerative disorders. Cell Metab. 30 (4), 630–655.
Lei, S., Zavala-Flores, L., Garcia-Garcia, A., Nandakumar, R., Huang, Y., Madayiputhiya, N., Stanton, R.C., Dodds, E.D., Powers, R., Franco, R., 2014. Alterations in energy/redox metabolism induced by mitochondrial and environmental toxins: a specific role for glucose-6-phosphate-dehydrogenase and the pentose phosphate pathway in paraquat toxicity. ACS Chem. Biol. 9 (9), 2032–2048.
Li, H., Sun, B., Huang, Y., Zhang, J., Xu, X., Shen, Y., Chen, Z., Yang, J., Shen, L., Hu, Y., Gu, H., 2022. Gene therapy of yeast NDI1 on mitochondrial complex I dysfunction in rotenone-induced Parkinson's disease models in vitro and vivo. Mol. Med. 28 (1), 456.
Liti, G., Carter, D.M., Moses, A.M., Warringer, J., Parts, L., James, S.A., Davey, R.P., Roberts, I.N., Burt, A., Koufopanou, V., Tsai, I.J., Bergman, C.M., Bensasson, D., O'Kelly, M.J.T., van Oudenaarden, A., Barton, D.B.H., Bailes, E., Nguyen, A.N., Jones, M., Quail, M.A., Goodhead, I., Sims, S., Smith, F., Blomberg, A., Durbin, R., Louis, E.J., 2009. Population genomics of domestic and wild yeasts. Nature 458, 337–341.
Lovejoy, P.C., Foley, K.E., Conti, M.M., Meadows, S.M., Bishop, C., Fiumera, A.C., 2021. Genetic basis of susceptibility to low-dose paraquat and variation between the sexes in Drosophila melanogaster. Mol. Ecol. 30, 2040–2053.
Marcireau, C., Joets, J., Pousset, D., Guilloton, M., Karst, F., 1996. FEN2: a gene implicated in the catabolite repression-mediated regulation of ergosterol biosynthesis in yeast. Yeast 12, 531–539.
Mendes-Ferreira, A., Sampaio-Marques, B., Barbosa, C., Rodrigues, F., Costa, V., Mendes-Faia, A., Ludovico, P., Leão, C., 2010. Accumulation of non-superoxide anion reactive oxygen species mediates nitrogen-limited alcoholic fermentation by Saccharomyces cerevisiae. Appl. Environ. Microbiol. 76, 7918–7924.
Mikawa, T., Kanoh, J., Ishikawa, F., 2010. Fission yeast Vps1 and Atg8 contribute to oxidative stress resistance. Genes Cells 15, 229–242.
Mülleder, M., Capuano, F., Pir, P., Christen, S., Sauer, U., Oliver, S.G., Ralser, M., 2012. A prototrophic deletion mutant collection for yeast metabolomics and systems biology. Nat. Biotechnol. 30, 1176–1178.
Naspolini, N.F., Rieg, C.E.H., Cenci, V.H., Cattani, D., Zamoner, A., 2021. Paraquat induces redox imbalance and disrupts glutamate and energy metabolism in the hippocampus of prepubertal rats. NeuroToxicology 85, 121–132.
Ngo, K.J., Paul, K.C., Wong, D., Kusters, C.D.J., Bronstein, J.M., Ritz, B., Fogel, B.L., 2024. Lysosomal genes contribute to Parkinson's disease near agriculture with high intensity pesticide use. NPJ Park. Dis. 10, 87.
Pascua-Maestro, R., Diez-Hermano, S., Lillo, C., Ganfornina, M.D., Sanchez, D., 2017. Protecting cells by protecting their vulnerable lysosomes: Identification of a new mechanism for preserving lysosomal functional integrity upon oxidative stress. PLoS Genet. 13, e1006603.
Paul, K.C., Cockburn, M., Gong, Y., Bronstein, J., Ritz, B., 2024. Agricultural paraquat dichloride use and Parkinson's disease in California's Central Valley. Int. J. Epidemiol. 53. https://doi.org/10.1093/ije/dyae004.
Pretty, J., Bharucha, Z.P., 2015. Integrated Pest Management for Sustainable Intensification of Agriculture in Asia and Africa. Insects 6, 152–182.
Quispe, X., Tapia, S.M., Villarroel, C., Oporto, C., Abarca, V., García, V., Martínez, C., Cubillos, F.A., 2017. Genetic basis of mycotoxin susceptibility differences between budding yeast isolates. Sci. Rep. 7, 9173.
Rego, A., Mendes, F., Costa, V., Chaves, S.R., Côrte-Real, M., 2020. Pkh1p-Ypk1p and Pkh1p-Sch9p pathways are activated by acetic acid to induce a mitochondrial-dependent regulated cell death. Oxid. Med. Cell. Longev. 2020, 7095078.

Robak, L.A., Jansen, I.E., van Rooij, J., Uitterlinden, A.G., Kraaij, R., Jankovic, J., 2017. International Parkinson's Disease Genomics Consortium (IPDGC), Heutink, P., Shulman, J.M. Excessive Burd. lysosomal Storage Disord. gene Var. Park. Dis. Brain 140, 3191–3203.

Rubilar, J.C., Outeiro, T.F., Klein, A.D., 2024. The lysosomal β-glucocerebrosidase strikes mitochondria: implications for Parkinson's therapeutics. Brain 147, 2610–2620. https://doi.org/10.1093/brain/awae070.

Sabir, M.S., Makarious, M.B., Huizing, M., Gahl, W.A., Platt, F.M., Malicdan, M.C.V., 2025. Comprehensive analysis of SLC17A5 variants in large European cohorts reveals no association with Parkinson's disease risk. Park. Relat. Disord. 134, 107790.

Saldaña, C., Villava, C., Ramírez-Villarreal, J., Morales-Tlalpan, V., Campos-Guillen, J., Chávez-Servín, J., García-Gasca, T., 2021. Rapid and reversible cell volume changes in response to osmotic stress in yeast. Braz. J. Microbiol 52, 895–903.

Salinas, F., de Boer, C.G., Abarca, V., García, V., Cuevas, M., Araos, S., Larrondo, L.F., Martínez, C., Cubillos, F.A., 2016. Natural variation in non-coding regions underlying phenotypic diversity in budding yeast. Sci. Rep. 6, 21849.

Schneider, C.A., Rasband, W.S., Eliceiri, K.W., 2012. NIH Image to ImageJ: 25 years of image analysis. Nat. Methods 9, 671–675.

See, W.Z.C., Naidu, R., Tang, K.S., 2022. Cellular and molecular events leading to paraquat-induced apoptosis: mechanistic insights into Parkinson's disease pathophysiology. Mol. Neurobiol. 59, 3353–3369.

Seeley, E.S., Kato, M., Margolis, N., Wickner, W., Eitzen, G., 2002. Genomic analysis of homotypic vacuole fusion. Mol. Biol. Cell 13, 782–794.

Sillapawattana, P., Gruhlke, M.C.H., Seiler, T.-B., Klungsupya, P., Charerntantanakul, W., 2024. Oxidative stress related effect of xenobiotics on eukaryotic model organism, Saccharomyces cerevisiae. Free Radic. Biol. Med. 212, 149–161.

Takahashi, K., Iwaoka, K., Takahashi, K., Suzuki, Y., Taguchi, K., Yamahara, K., Maeda, T., 2021. Cerebrospinal fluid levels of oxidative stress measured using diacron-reactive oxygen metabolites and biological antioxidant potential in patients with Parkinson's disease and progressive supranuclear palsy. Neurosci. Lett. 757, 135975.

Zheng, Y., Li, M., Chen, X.-, Zheng, Z., Chen, Z., Tian, R., Zhao, Y.G., 2025. SOD1 is delivered to lysosomes via autophagy to maintain lysosomal function and integrity. J. Cell Biol. 224, e202501007.

Zwietering, M.H., Jongenburger, I., Rombouts, F.M., van 't Riet, K., 1990. Modeling of the bacterial growth curve. Appl. Environ. Microbiol. 56, 1875–1881.